SARS-CoV-2 causes a specific dysfunction of the kidney proximal tubule

Check for updates

Alexis Werion[1,11], Leila Belkhir[2,3,11], Marie Perrot[1], Gregory Schmit[4,5], Selda Aydin[3,4], Zhiyong Chen[6], Andrea Penaloza[7], Julien De Greef[2,3], Halil Yildiz[2,3], Lucie Pothen[2,3], Jean Cyr Yombi[2,3], Joseph Dewulf[4], Anais Scohy[4], Ludovic Gérard[3,8], Xavier Wittebole[3,8], Pierre-François Laterre[3,8], Sara E. Miller[9], Olivier Devuyst[1,3,6,12], Michel Jadoul[1,7,12] and Johann Morelle[1,3,12]; on behalf of the Cliniques universitaires Saint-Luc (CUSL) COVID-19 Research Group[10]

[1]Division of Nephrology, Cliniques universitaires Saint-Luc, Brussels, Belgium; [2]Division of Internal Medicine and Infectious Diseases, Cliniques universitaires Saint-Luc, Brussels, Belgium; [3]Institut de Recherche Expérimentale et Clinique, UCLouvain, Brussels, Belgium; [4]Department of Laboratory Medicine, Microbiology and Pathology, Cliniques universitaires Saint-Luc, Brussels, Belgium; [5]Centre of Forensic Medicine, Cliniques universitaires Saint-Luc, Brussels, Belgium; [6]Department of Physiology, Mechanisms of Inherited Kidney Disorders Group, University of Zurich, Zurich, Switzerland; [7]Department of Emergency Medicine, Cliniques universitaires Saint-Luc, Brussels, Belgium; [8]Department of Intensive Care Medicine, Cliniques universitaires Saint-Luc, Brussels, Belgium; and [9]Department of Pathology, Duke University Medical Center, Durham, North Carolina, USA

Coronavirus disease 2019 (COVID-19) is commonly associated with kidney damage, and the angiotensin converting enzyme 2 (ACE2) receptor for SARS-CoV-2 is highly expressed in the proximal tubule cells. Whether patients with COVID-19 present specific manifestations of proximal tubule dysfunction remains unknown. To test this, we examined a cohort of 49 patients requiring hospitalization in a large academic hospital in Brussels, Belgium. There was evidence of proximal tubule dysfunction in a subset of patients with COVID-19, as attested by low-molecular-weight proteinuria (70-80%), neutral aminoaciduria (46%), and defective handling of uric acid (46%) or phosphate (19%). None of the patients had normoglycemic glucosuria. Proximal tubule dysfunction was independent of pre-existing comorbidities, glomerular proteinuria, nephrotoxic medications or viral load. At the structural level, kidneys from patients with COVID-19 showed prominent tubular injury, including in the initial part of the proximal tubule, with brush border loss, acute tubular necrosis, intraluminal debris, and a marked decrease in the expression of megalin in the brush border. Transmission electron microscopy identified particles resembling coronaviruses in vacuoles or cisternae of the endoplasmic reticulum in proximal tubule cells. Among features of proximal tubule dysfunction, hypouricemia with inappropriate uricosuria was independently associated with disease severity and with a significant increase in the risk of respiratory failure requiring invasive mechanical ventilation using Cox (adjusted hazard ratio 6.2, 95% CI 1.9-20.1) or competing risks (adjusted sub-distribution hazard ratio 12.1, 95% CI 2.7-55.4) survival models. Thus, our data establish that SARS-CoV-2 causes specific manifestations of proximal tubule dysfunction and provide novel insights into COVID-19 severity and outcome.

The recent pandemic of coronavirus disease 2019 (COVID-19) caused by the severe acute respiratory syndrome coronavirus-2 (SARS-CoV-2) has major public health and economic impact.[1] The clinical spectrum of COVID-19 is broad, ranging from asymptomatic carrier state to severe, bilateral, and diffuse pneumonia, potentially leading to acute respiratory distress syndrome (ARDS), respiratory failure, and/or multiple organ dysfunction.[2,3] Identifying early manifestations of COVID-19 and patients at risk for disease progression and respiratory failure is of crucial importance to alleviate the major stress on healthcare systems.

The angiotensin-converting enzyme 2 (ACE2), the receptor mediating the entry of SARS-CoV-2 in human cells, is expressed in the lung, heart, intestine, and kidney, providing a rationale for the systemic manifestations of the disease.[4–7] Increasing evidence suggests that COVID-19 may cause kidney damage, as indicated by the occurrence of proteinuria, hematuria, and elevated serum creatinine level on admission; the high incidence of acute kidney injury; and a spectrum of pathologic abnormalities including acute tubular necrosis,

Correspondence: Johann Morelle, Division of Nephrology, Cliniques universitaires Saint-Luc, Avenue Hippocrate 10, B-1200 Brussels, Belgium. E-mail: johann.morelle@uclouvain.be

[10]See Appendix for list of Cliniques universitaires Saint-Luc COVID-19 Research Group participants.

[11]AW and LB contributed equally to this work.

[12]OD, MJ, and JM contributed equally as co-directors of the study.

Table 1 | Baseline characteristics of the 49 patients with specific urinalysis

Demographics and comorbidities	n = 49
Age, yr	64 (54–74)
Male gender	34 (69)
Ethnicity	
Caucasian	42 (86)
Sub-Saharan African	6 (12)
Other	1 (2)
Cardiovascular disease	9 (18)
Chronic kidney disease	7 (14)
Hypertension	23 (47)
Diabetes	10 (20)
Human immunodeficiency virus infection	0 (0)
Chronic liver disease	1 (2)
Chronic pulmonary disease	5 (12)
Medications	
Allopurinol or febuxostat	4 (8)
Angiotensin receptor blocker	10 (20)
ACE inhibitor	10 (20)
Chronic immunosuppressive treatment[a]	4 (8)
Anti-cancer drugs[b]	4 (8)
Symptoms and vitals at admission	
Duration of symptoms, d	7 (3–9)
Symptoms at admission	
Fever	39 (80)
Cough	29 (59)
Dyspnea	35 (71)
Sore throat	2 (4)
Confusion	6 (12)
Anosmia/ageusia	6 (12)
Rhinitis	7 (14)
Diarrhea	14 (29)
Chest pain	4 (8)
Admission via emergency department	47 (96)
Sa02, %	92 (87–96)
Systolic BP, mm Hg	139 (126–150)
Diastolic BP, mm Hg	75 (69–82)
Heart rate, bpm	93 (88–103)
Lab tests and dipstick urinalysis at admission	
hsCRP, mg/l	105 (54–146)
Glycemia, mg/dl	121 (109–146)
Serum creatinine, mg/dl	1.0 (0.8–1.2)
eGFR, ml/min per 1.73 m^2	72 (54–92)
Serum uric acid, mg/dl	4.9 (3.3–5.9)
Sodium, mmol/l	135 (133–138)
Bicarbonate, mmol/l	23 (22–25)
AST, IU/l	36 (24–53)
ALT, IU/l	27 (17–46)
Total bilirubin, mg/dl	0.5 (0.4–0.7)
CK, IU/l	119 (74–211)
LDH, IU/l	356 (279–491)
Lymphocytes, n/μl	650 (500–1060)
Platelets, 10^3/μl	203 (131–233)
Dipstick proteinuria, n = 43	
0	8 (19)
1+	13 (30)
2+	19 (44)
3+	3 (7)
Computed tomography scan of the chest upon admission	
Extent of lesions on chest CT scan, %, n = 45	
<10	4 (9)
10–25	18 (40)
25–50	14 (31)
>50	9 (20)
Drugs received for COVID-19	
Hydroxychloroquine	48 (98)
Azithromycin	7 (14)

Table 1 | (Continued)

Demographics and comorbidities	n = 49
Antiviral drugs	0 (0)
Immunomodulatory drugs[c]	16 (33)

ACE, angiotensin-converting enzyme; ALT, alanine aminotransferase; AST, aspartate aminotransferase; BP, blood pressure; bpm, beats per minute; CK, creatine kinase; COVID-19, coronavirus disease 2019; CT, computed tomography; eGFR, Chronic Kidney Disease–Epidemiology Collaboration (CKD-EPI) estimated glomerular filtration rate; hsCRP, highly-sensitive C-reactive protein; LDH, lactate dehydrogenase; Sa02, oxygen saturation while breathing ambient air.
[a]Chronic immunosuppressive treatment included (one or more per patient) ciclosporin A (1), corticosteroids (2), methotrexate (1), rituximab (1).
[b]Anti-cancer drugs included cyclophosphamide (1), doxorubicine (1), vincristine (1), venetoclax (1), cisplatin (1), and cytarabine (1).
[c]Immunomodulatory drugs for COVID-19 (one or more per patient) included corticosteroids (7), interleukin-7 (8), and tocilizumab (1).
Continuous variables are expressed as median (interquartile range), and categorical variables as n and (%).

endothelial damage and capillary occlusions, deposition of complement complex on tubules, and glomerular lesions identified in autopsy reports.[8–13] Kidney damage may result from hemodynamic factors, dysfunctional immune responses,[14] or direct viral infection of kidney cells, the latter being compatible with the detection of SARS-CoV-2 mRNA and protein in glomerular and tubular cells[15] and of purported viral particles in podocytes and proximal tubule (PT) cells.[8,16,17] However, the identification of viral particles by electron microscropy is challenging, as they may easily be mistaken for normal cell organelles such as the endoplasmic reticulum (ER), clathrin-coated vesicles, or multivesicular bodies.[18–20]

Overall, several arguments suggest that the PT may be a specific target for SARS-CoV-2 infection. Here, we analyzed the characteristics, extent, and structural correlates of PT dysfunction in a cohort of patients admitted with SARS-CoV-2 infection in a large academic hospital in Brussels, Belgium. We further investigated the association of various markers of PT dysfunction with COVID-19 severity and outcome.

RESULTS
Study population
The detection of proteinuria of unknown mechanism by routine analysis among ∼80% of patients in the early phase of the pandemic prompted us to perform specific urinalyses in 49 patients with documented SARS-CoV-2 infection hospitalized at the Cliniques universitaires Saint-Luc in Brussels, Belgium, between March 31, 2020 and April 18, 2020 (Supplementary Figure S1). Patients on chronic kidney replacement therapy at the time of admission were excluded.

Baseline characteristics of the 49 patients with specific urinalysis are presented in Table 1. Median age (interquartile range [IQR]) at admission was 64 years (54–74 years); 69% were male, 86% were of Caucasian origin, and 12% were of Sub-Saharan African origin. A total of 18%, 47%, 20%, and 14% had a history of cardiovascular disease, hypertension, diabetes, and chronic kidney disease, respectively. Chronic kidney disease was ascribed to hypertension (n = 2; 29%),
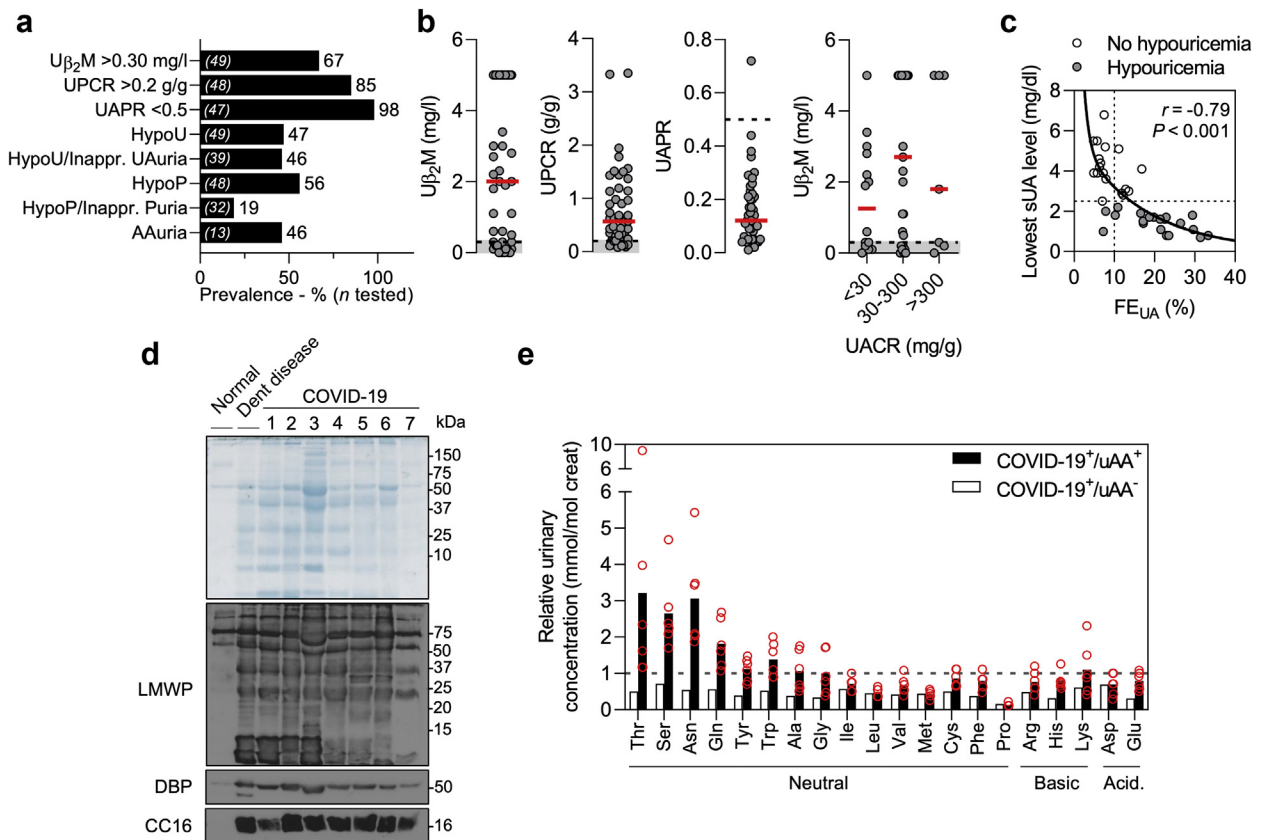
Figure 1 | Proximal tubule dysfunction in patients with coronavirus disease 2019 (COVID-19). (**a**) Prevalence (%) of signs of proximal tubule (PT) dysfunction in patients with active COVID-19. Numbers (n) of patients tested are shown in brackets inside the bars. (**b**) Distribution of urinary β_2-microglobulin (Uβ_2M), urinary protein-to-creatinine ratio (UPCR), and urinary albumin-to-protein ratio (UAPR), and relationship between Uβ_2M and urinary albumin-to-creatinine ratio in patients with COVID-19. Circles represent individual values, and red lines represent medians. (**c**) Inverse relationship between the lowest serum uric acid (sUA) level and fractional excretion of uric acid (FE$_{UA}$) in patients with (gray circles) versus without (open circles) hypouricemia. Spearman's coefficient $r = -0.79$ (95% confidence interval -0.89, -0.63), $P < 0.001$, n = 39. (**d**) Sodium dodecyl sulfate polyacrylamide gel electrophoresis followed by Coomassie blue staining and immunoblot shows the presence of low-molecular weight proteins (LMWP), vitamin D binding protein (DBP), and Clara cell secretory protein (CC16). Normal urine and urine from a patient with Dent disease (a rare inherited PT dysfunction caused by *CLCN5* mutation) are shown as controls. Molecular weights (in kDa) of the urinary proteins are provided. (**e**) Relative urinary concentration of amino acids in patients with COVID-19 and aminoaciduria (COVID-19$^+$/uAA$^+$; black bars) or no aminoaciduria (COVID-19$^+$/uAA$^-$; open bars). The reference corresponds to the upper limit of normal. Individual values are represented by circles, and bars represent the mean values. AAuria; aminoaciduria; creat, creatinine; HypoP, hypophosphatemia; HypoU, hypouricemia; inappr. Puria, inappropriate phosphaturia; inappr. UAuria, inappropriate uricosuria. Ala, alanine; Arg, arginine; Asn, asparagine; Asp, aspartate; Cys, cysteine; Gln, glutamine; Glu, glutamate; Gly, glycine; His, histidine; Ile, isoleucine; Leu, leucine; Lys, lysine; Met, methionine; Phe, phenylalanine; Pro, proline; Ser, serine; Thr, threonine; Trp, tryptophan; Tyr, tyrosine; Val, valine. To optimize viewing of this image, please see the online version of this article at www.kidney-international.org.

chronic interstitial nephritis (n = 2; 29%), nephron mass reduction (n = 1; 14 %), or unknown origin (n = 2; 29%). Forty percent were treated with a renin–angiotensin system inhibitor. Eight percent were on chronic immunosuppressive treatment, and another 8% were on anti-cancer therapy. A detailed list of these medications is provided in Table 1.

Patients were admitted a median (IQR) of 7 days (3–9 days) after the onset of symptoms, mainly with fever (80%), dyspnea (71%), and cough (59%; Table 1). Almost all patients (47 of 49; 96%) were admitted via the emergency room. At admission, median oxygen saturation while breathing ambient air was 92% (87%–96%); highly sensitive C-reactive protein was 105 mg/l (54–146); glomerular filtration rate estimated by the Chronic Kidney Disease–Epidemiology

Collaboration equation (eGFR) was 72 ml/min per 1.73 m^2 (54–92); and lymphocyte count was 650 per μl (500–1060). The extent of pulmonary lesions at admission, quantified using computed tomography,[21] was as follows: <10% for 9% of the patients; 10%–25% for 40%; 25%–50% for 31%; and >50% for 20%. Most patients were hospitalized in dedicated COVID-19 units (n = 40; 82%), while a minority (n = 9; 18%) were directed to a dedicated intensive care unit. During hospitalization, 48 patients (98%) received hydroxychloroquine, and 16 (33%) received immunomodulatory drugs for COVID-19. No patient was treated with antiviral drugs (Table 1). The 166 patients with routine urinalysis only who presented between February 23, 2020 and April 18, 2020 had similar baseline characteristics (Supplementary Table S1).

Table 2 | Prevalence of proximal tubule dysfunction in COVID-19

Markers of PT dysfunction	n tested	n positive (%)
Urinary β_2-microglobulin >0.30 mg/l	49	33 (67)
Urinary protein-to-creatinine ratio >0.2 g/g	48	41 (85)
Urinary albumin-to-protein ratio <0.5	47	46 (98)
Hypouricemia	49	23 (47)
With inappropriate uricosuria	39	18 (46)
Hypophosphatemia	48	27 (56)
With inappropriate phosphaturia	32	6 (19)
Aminoaciduria	13	6 (46)
LMW proteinuria on SDS-PAGE	15	10 (67)
Normoglycemic glucosuria	43	0 (0)

COVID-19, coronavirus disease 2019; LMW, low molecular weight; SDS-PAGE, sodium dodecyl sulfate polyacrylamide gel electrophoresis.
Hypouricemia with inappropriate uricosuria is defined as serum uric acid <2.5 mg/dl and fractional excretion of uric acid >10%; and inappropriate phosphaturia is defined as serum phosphate <0.81 mmol/l and a fractional excretion of phosphate >20%.

PT dysfunction in COVID-19

Specific urinalyses, performed a median (IQR) of 9 days (3–16) after admission, assessed the occurrence and pattern of PT dysfunction in patients with COVID-19 (Figure 1; Table 2; Supplementary Figure S2). Among the 49 COVID-19 patients, 69% (33 of 49) had elevated urinary levels of β_2-microglobulin; 85% (41 of 48 tested) had a urinary protein-to-creatinine ratio (UPCR) >0.2 g/g; and 98% (46 of 47) had a urinary albumin-to-protein ratio <0.5 (Figure 1a and b; Table 2). Electrophoresis of urine samples from COVID-19 patients evidenced multiple protein bands below 70 kDa (low-molecular-weight [LMW] proteinuria), which included the vitamin D–binding protein (DBP) and Clara cell secretory protein (CC16). These bands, which were not detected in healthy controls, are similar to those detected in the urine of patients with congenital PT dysfunction due to Dent disease, toxic acute tubular necrosis secondary to tenofovir, or heavy proteinuria caused by nephrotic syndrome (Figure 1d; Supplementary Figure S3; Supplementary Table S2). The prevalence of proteinuria was similar between patients without versus with diabetes (UPCR >0.2 g/g: 84% vs. 90%, P = 0.64) and between patients without versus with history of chronic kidney disease (UPCR >0.2 g/g: 86% vs. 83%, P = 0.88). Heavy proteinuria (UPCR >2.5 g/g) was identified in 2 patients, and one had selective albuminuria (urinary albumin-to-protein ratio >0.5). The first had heavy proteinuria months before COVID-19, suggesting unrelated kidney disease, whereas no past urinalysis was available in the other.

Forty-seven percent (23 of 49) and 56% (27 of 48) of the patients had hypouricemia and/or hypophosphatemia, respectively (Figure 1a; Table 2). Inappropriate uricosuria (fractional excretion of uric acid >10%) was observed in 90% (18 of 20) of the patients with hypouricemia, and defective tubular handling of uric acid (hypouricemia with inappropriate uricosuria) was found in 46% (18 of 39 tested) of the cohort (Figure 1a; Figure 1c; Table 2). Hypophosphatemia with inappropriate phosphaturia (fractional excretion of phosphate >20%) was observed in 19% (6 of 32).

Aminoaciduria was detected in 6 of 13 (46%) tested COVID-19 patients (Figure 1a; Table 2) and was restricted to neutral amino acids (Figure 1e; Supplementary Table S3), a pattern similar to that found in Hartnup disease, caused by recessive mutations in *SLC6A19*, which encodes the sodium-dependent neutral amino acid transporter B^0AT1 (solute carrier family [SLC]6A19).[22,23] Of interest, B^0AT1 interacts with ACE2,[6,23] both highly expressed in PT cells of the normal human kidney (Supplementary Figure S4A, C, and D). Transcriptomic analysis of specific segments of the mouse nephron confirmed the enrichment of genes encoding for the SARS-CoV-2 receptor ACE2, its homologue TMEM27 (collectrin), uric acid transporter URAT1 (SLC22A12), sodium-dependent phosphate cotransporter NaPi-IIa (SLC34A1), and B_0AT1 in PT segments (Supplementary Figure S4B).

Three of the 43 patients tested had positive dipstick glucosuria upon admission. Two of them had a history of type 2 diabetes, concomitant hyperglycemia, and significant glucosuria (blood glucose 215 mg/dl and 331 mg/dl; and dipstick glucosuria 2+ and 4+, respectively), whereas the remaining individual had prediabetes (HbA1c 6.0%), slightly elevated blood glucose (127 mg/dl), and mild glucosuria (1+). In contrast with other signs of PT dysfunction, none of the patients in the cohort showed normoglycemic glucosuria (Table 2).

Altogether, these observations showed that a specific dysfunction of the PT develops in a subset of patients with severe forms of COVID-19, occurs early during the course of the disease, and is characterized by LMW proteinuria, defective handling of uric acid and phosphate, and neutral aminoaciduria.

PT dysfunction, clinical presentation, disease severity, and outcomes

To assess the potential clinical relevance of PT dysfunction in patients hospitalized with COVID-19, we compared the clinical presentation, disease severity, and outcomes of patients with versus without elevated urinary β_2-microglobulin, defective handling of uric acid and phosphate, or aminoaciduria (Supplementary Tables S4–S7).

Biological signs of PT dysfunction were not associated with demographics, disease presentation or severity, or viral load, estimated from real-time polymerase chain reaction and cycle threshold (Ct) values at admission. They were also independent from comorbidities and from medications interfering with uric acid production or with potential PT toxicity, including antiviral or immunomodulatory drugs (Table 1; Supplementary Table S1).

Patients with defective handling of uric acid (i.e., hypouricemia with inappropriate uricosuria) who also had higher prevalence of LMW proteinuria, aminoaciduria, and defective handling of phosphate (Supplementary Table S5) showed higher disease severity compared with others. This was evidenced by a lower nadir of lymphocyte count (median [IQR]: 250 per μl [100–360] vs. 500 per μl [280–910], P = 0.006),
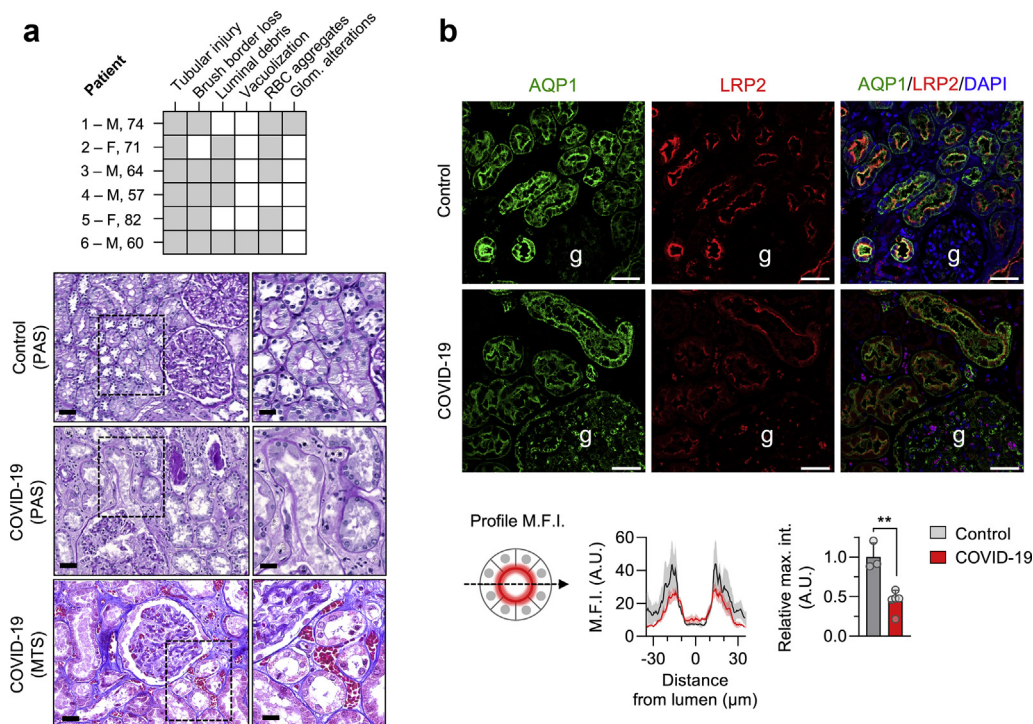
Figure 2 | Proximal tubule (PT) damage in kidneys of coronavirus disease 2019 (COVID-19) patients. (a) Pathologic scoring of kidney lesions in COVID-19. The grid summarizes pathologic findings on postmortem examination in 6 patients with COVID-19 and the presence (gray) or absence (white) of tubular injury, brush border loss, debris in the lumen, red blood cell (RBC) aggregates, vacuolization of tubular cells, and glomerular (glom.) alterations. Representative pictures of sections from control and COVID-19 kidneys, stained with periodic acid–Schiff (PAS) or Masson's trichrome staining (MTS), show prominent tubular lesions with dilation, mitoses in epithelial cells, major alterations of the brush border (i.e., in the S1 segment of the PT), shedding of cellular debris into the lumen, as well as erythrocytes aggregates in peritubular capillaries. Original magnification ×20 and ×40; bars = 50 μm and 25 μm, on left and right pictures, respectively. **(b)** Representative pictures of double immunostaining with anti-aquaporin (AQP) 1 (green channel) and anti-megalin (low-density lipoprotein receptor–related protein [LRP] 2, red channel) antibodies viewed under confocal fluorescence microscopy in kidney sections from a control and a patient with COVID-19. Nuclei are stained with 4′,6-diamidino-2-phenylindole (DAPI; blue channel). Original magnification ×20. Bars = 50 μm. Mean fluorescence intensity (M.F.I.) profiles and relative maximal intensity (max. int.) for LRP2 were quantified on cross sectional sections of PT from 3 controls (gray) and 5 patients who died of COVID-19 (red). Data are mean values and SEM. $P = 0.002$, unpaired t test. M, male; F, female. To optimize viewing of this image, please see the online version of this article at www.kidney-international.org.

and higher peak values of highly sensitive C-reactive protein (324 mg/dl [243–349] vs. 126 mg/dl [51–245], $P = 0.002$), lactate dehydrogenase (584 IU/l [524–726] vs. 394 IU/l [317–466], $P < 0.001$), and D-dimers (4461 ng/ml [2098–13,348] vs. 1234 ng/ml [753–2827], $P = 0.001$), in these patients compared to those without inappropriate uricosuria (Supplementary Table S5).

During a median follow-up (IQR) of 44 days (31–56), 19 of 49 patients (39%) in the cohort required invasive mechanical ventilation, 14 (29%) died, 11 (22%) developed acute kidney injury, and 2 (4%) required kidney replacement therapy (Supplementary Figure S1; Supplementary Table S1). Hypouricemia with inappropriate uricosuria was associated with a higher occurrence of invasive mechanical ventilation (83% vs. 14%, $P < 0.001$) and death (50% vs. 14%, $P = 0.02$) and with longer hospital stay (27 days [17–46] vs. 12 [6–17], $P < 0.001$), compared to patients with normal tubular handling of uric acid (Supplementary Table S5). Time-to-event analyses using Cox regressions showed an independent association between defective tubular handling of uric

acid and higher risk of invasive mechanical ventilation or death (adjusted hazard ratio [HR] 6.2, 95% confidence interval 1.9–20.1, $P = 0.002$). An alternative approach considering death and discharge from hospital as competing events confirmed the independent association between tubular loss of uric acid and the need for invasive mechanical ventilation (adjusted subdistribution HR 12.1, 95% confidence interval 2.7–55.4, $P = 0.001$; Supplementary Table S8).

PT damage in kidneys of COVID-19 patients

To characterize structural alterations associated with PT dysfunction, we analyzed 6 kidney autopsy samples from patients who died of COVID-19, for whom tissue samples were well preserved with absence of autolysis at the optical level. Patient age ranged between 57 and 82 years; 4 were male; all had abnormal proteinuria, and 2 developed acute kidney injury requiring kidney replacement therapy (Supplementary Table S9). None of the patients received antiviral medications.
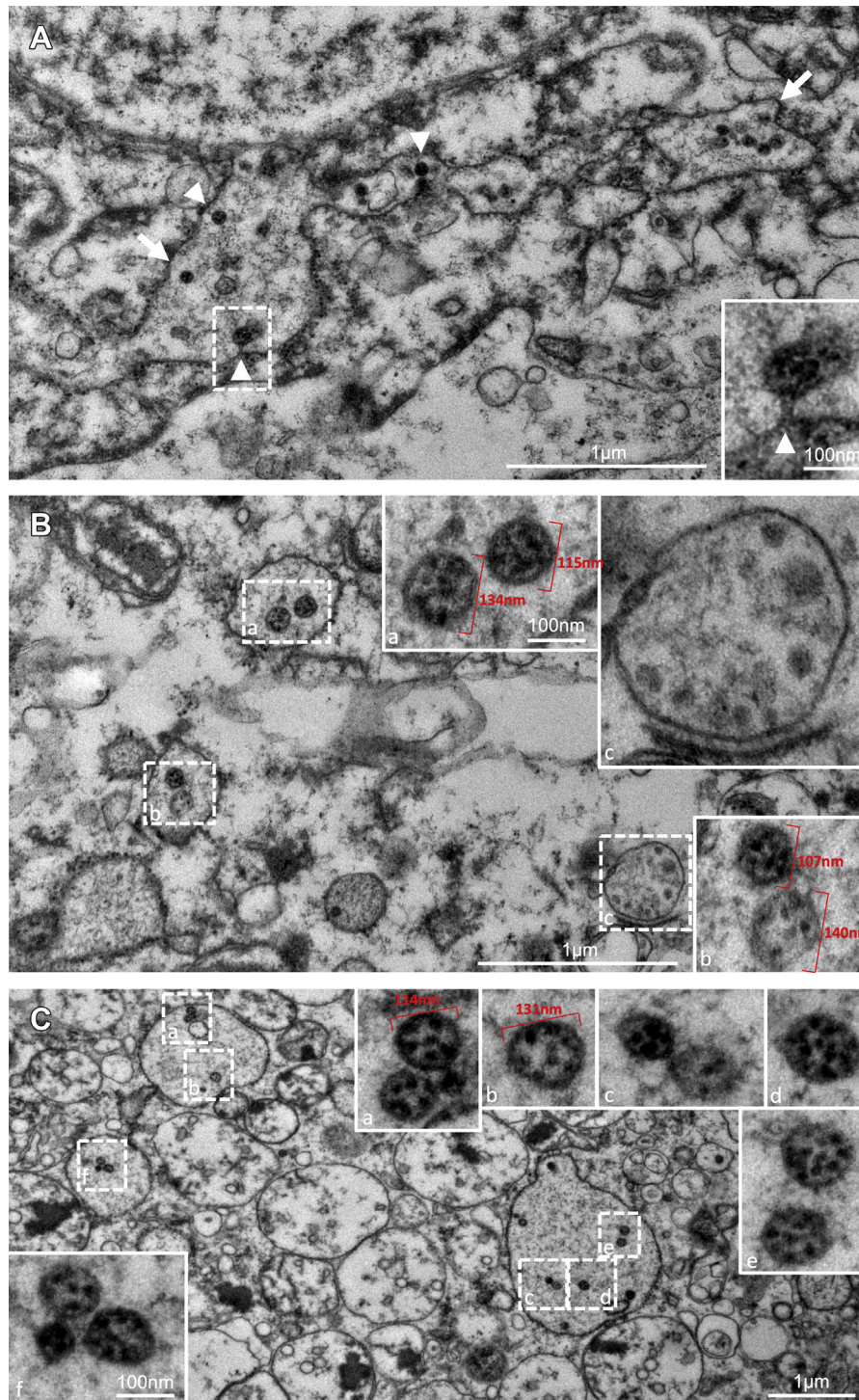
Figure 3 | Transmission electron microscopy of particles in proximal tubule cells in a kidney sample of an autopsied patient deceased from coronavirus disease 2019 (COVID-19). (**A**) Low-magnification electron microscopy image showing numerous particles of approximately 90–140 nm in diameter within the lumen of rough endoplasmic reticulum (RER) (arrows), some of which have budded into the lumen from the cytoplasm (arrowheads). Inset (**a**) shows the budding and the stalk of a particle. Size is indicated by the magnification bars. (**B**) Particles observed inside vacuoles formed by RER and lighter densities inside smooth endoplasmic reticulum. Areas seen in the lower magnification marked by dashed-line boxes are enlarged in solid-line insets and are labeled correspondingly. Insets (**a**) and (**b**) are representative of numerous particles containing dense smudgy dots in similarly sized particles observed within RER elsewhere. In some particles (inset **a**), the trilaminar membrane envelope is evident. A larger vacuole (inset **c**) without ribosomes studding the outside and located near the Golgi apparatus contains irregularly sized densities and does not contain viruses. Size of the low magnification is indicated on the print; size in the high magnifications is the same in all insets and is indicated by the bar in inset (**a**). (**C**) Particles shown (similarly to those in **B** above) at low magnification in the large image in dashed-line boxes and at high magnification in solid-line insets corresponding to the dashed-line boxes (**a–f**). All particles have irregular dense black dots inside, and a few (e.g., see insets **b** and **e**) have crisp small rings, possibly exact cross sections of tubular or helical structures. (Continued)

Postmortem examination of the COVID-19 kidneys showed prominent and diffuse PT damage in all patients, with dilation of the tubular lumen containing cellular debris, denuded basement membranes, and major alterations of the brush border (Figure 2a; Supplementary Figure S5; Supplementary Table S10). In addition to tubular lesions, erythrocyte aggregates in peritubular and/or glomerular capillaries were found in 5 of the 6 patients. One patient with moderate proteinuria (UPCR 0.7 g/g) showed a single lesion of focal and segmental glomerulosclerosis (tip lesion variant). Focal infiltration of the interstitium by mononuclear cells was observed in 2 of the 6 patients.

Confocal microscopy examination revealed that the expression of the multi-ligand receptor megalin (LRP2), which mediates the reabsorption of LMW proteins at the apical membrane of PT cells, was severely decreased (∼50%) in the PT cells of patients with COVID-19, compared to the normal kidney (Figure 2b). The decreased expression of megalin contrasted with the stable (trend to increased) expression of ACE2 in PT cells of COVID-19 kidneys (Supplementary Figure S4A).

Transmission electron microscopy identified particles resembling coronaviruses in vacuoles or cisternae of the ER in PT cells (Figure 3). They measured between 90 and 140 nm and contained small dense irregular dots of 10–20 nm. Some particles were budding into the ER lumen, and a few had faint wisps of projections on their surfaces that contacted the luminal contents, not the cytoplasm. A trilaminar envelope was identified around some particles. Some of the particles contained a few (1 to 3) crisp, dense circles of 10–15 nm. Ultrastructurally, the tissue was degraded, as expected from the pathology observations.

DISCUSSION

In this cohort of patients hospitalized for SARS-CoV-2 infection, we provide direct evidence that PT dysfunction develops in a subset of patients with COVID-19 and is characterized by LMW proteinuria, hypophosphatemia, and hypouricemia due to inappropriate urinary loss of phosphate and uric acid, and neutral aminoaciduria. The PT dysfunction is independent from preexisting kidney disease, glomerular proteinuria, viral load, or toxic medications. Defective tubular handling of uric acid is independently associated with disease severity and with a higher incidence of respiratory failure requiring mechanical ventilation. Analyses of autopsy kidney samples revealed tubular damage, defective expression of megalin, and presence of particles resembling coronaviruses in vacuoles or ER cisternae in PT cells.

Our data document that COVID-19 causes a specific dysfunction of the PT. The PT cells reabsorb a large amount of ions, solutes, and LMW proteins, using specialized transport systems that operate in their apical membrane.[24] These

transport systems include multi-ligand receptors such as megalin, the urate transporter URAT1 (SLC22A12), the sodium-dependent phosphate cotransporters NaPi-IIa (SLC34A1) and NaPi-IIc (SLC34A3), and amino acid transporters such as the sodium-dependent neutral amino acid transporter B^0AT1 (SLC6A19).[23,25,26] Impairment of PT transport processes leads to the urinary loss of LMW proteins and solutes (e.g., amino acids, uric acid, phosphate), a clinical entity called renal Fanconi syndrome. The PT dysfunction can result from inherited disorders (e.g., Dent disease, Lowe syndrome, cystinosis) or be acquired (monoclonal light chains, toxins, drugs, autoimmune disorders).[27] The PT dysfunction detected in patients with COVID-19 variably includes LMW proteinuria, aminoaciduria, and inappropriate urinary loss of uric acid and phosphate but not of glucose. This corresponds to a partial renal Fanconi syndrome, as observed in other PT disorders.[24,27–29] The molecular mechanisms accounting for such specific defects remain mostly unknown.

Postmortem examination of kidneys from patients with COVID-19 showed prominent lesions of PT injury, including loss of brush border, cell necrosis, and intraluminal debris, in line with previous reports.[16] These lesions are associated with an ∼50% reduction in the apical staining for megalin in PT cells. Studies in model organisms and congenital disorders including Donnai-Barrow syndrome, caused by mutations in the LRP2 gene coding for megalin, or Dent disease, caused by mutations in the CLCN5 gene coding for the endosomal chloride-proton exchanger ClC-5, have highlighted the critical role of megalin in the reabsorption of LMW ligands by PT cells.[24,25,30] Of note, alteration of megalin expression was also observed in patients with tenofovir-induced PT dysfunction,[31] confirming that the defect is not restricted to COVID-19. Conversely, the expression of megalin is preserved in patients presenting acute tubular injury without overt PT dysfunction, related, for example, to sepsis, aminoglycosides, or hepatorenal syndrome.[31]

The fact that PT cells highly express ACE2 suggests that they could be targeted by SARS-CoV-2 at an early stage of disease. The binding affinity of SARS-CoV-2 spike glycoprotein to ACE2 is a major determinant of disease severity.[32] Besides its role in the renin–angiotensin system, ACE2 facilitates the trafficking of B^0AT1 to the apical membrane.[23] Recent studies reported the cryo-electron microscopy structure of the full-length human ACE2, forming heterodimers with B^0AT1.[6] The aminoaciduria observed in patients with COVID-19 is essentially composed of neutral amino acids, similar to that encountered in patients with Hartnup disorder, caused by recessive, loss-of-function mutations in B^0AT1. As B^0AT1 requires ACE2 (or the related protein collectrin) for its apical targeting in epithelial cells, one could speculate that

---

Figure 3 | (Continued) Size of the low magnification is indicated on the print; size in the high magnifications is the same in all insets and is indicated by the bar in inset (f). To optimize viewing of this image, please see the online version of this article at www.kidney-international.org.

SARS-CoV-2 binding and entry may lead to a partial dysfunction of the amino acid transporter, causing mild neutral aminoaciduria. The fact that B^0AT1 is not directly affected by SARS-CoV-2 explains the moderate loss in patients with COVID-19 compared to Hartnup disease. The downregulation of specific tubule transporters, including URAT1, caused by viral mimetics in experimental models, also supports a causative link between infection and PT dysfunction.[33]

SARS-CoV-2 may damage the kidney by various mechanisms, including direct viral infection. The presence of SARS-CoV-2 RNA and shedding of viable SARS-CoV-2 in the urine have been reported.[34,35] SARS-CoV-2 is able to infect human kidney organoids expressing ACE2 and PT cell markers, with inhibition by soluble recombinant human ACE2.[36] Particles resembling coronavirus have been described in kidney samples from autopsied COVID-19 patients.[16,17,37] Several articles have refuted these data, and these structures have been identified as clathrin-coated vesicles or multivesicular bodies.[19,20] The particles shown here are uniform in size and appearance, are of the right size (90–140 nm), and have similar morphology to coronaviruses. They are located inside vacuoles or ER lumens and show faint hints of projections in contact with the vacuolar contents—not the cell cytoplasm.[19] Also, the particles contain dense dots (10–15 nm), forming either crisp circles or larger, smudgy dots, that may correspond to sections across the tube- or helix-forming of the virus nucleocapsid.[38,39] Of note, most dots inside these particles appear larger than nucleocapsids observed in properly fixed tissue cultures.[38,39] These dots are approximately the size of ribosomes ($\sim$20 nm); however, only arenaviruses appear to contain ribosomes, and to our knowledge, no normal cell structures appear like this. Alternatively, the larger-than-expected (for a nucleocapsid) and irregularly shaped dense dots could be related to poor fixation and delay in processing.[38,39]

In cells containing these virus-like structures, the particles are more uniform in size than any normal cell architecture, such as secretory granules, and they do not have the solid dark center of dense granules. With the limitations stated above, we believe that identified particles resemble viruses in most respects and are possible candidates for coronaviruses in PT cells. Because many intracellular particles can masquerade as viruses,[40,41] further analyses, including immunoelectron microscopy, are necessary to prove their identification as viruses.

Despite the small cohort size, our observations suggest that the presence of hypouricemia due to impaired tubular handling of uric acid, a marker of PT dysfunction, is associated with disease severity and outcomes, in particular the need for invasive mechanical ventilation. Interestingly, hypouricemia, was common and associated with poor outcome in patients with SARS.[42] Potential mechanisms linking PT dysfunction and respiratory failure may include the loss of important solutes, including uric acid, which may affect defense against oxidative stress and respiratory

function.[43] Genetic factors regulating SARS-CoV-2 entry into host cells may also contribute to multi-organ severity in COVID-19. Of note, we did not observe any association between PT dysfunction and viral load, nephrotoxic medications, or comorbidities. Finally, although almost all patients were given the drug, hydroxychloroquine does not cause PT toxicity. If these findings are validated, markers of PT dysfunction might be useful for the initial work-up of COVID-19 patients and for identifying patients at risk for progression to severe disease.

The strengths of this study include the availability of a large cohort of well characterized patients admitted via the emergency room; standardized protocols of treatment; detailed characterization of PT dysfunction; outcome analysis; correlations with viral load; and analyses on kidney samples from patients with COVID-19. Our work also has limitations, including the lack of standardized characterization of PT markers in all patients at admission, with a limited number of measurements for some markers, as well as the single-center design of the study, requiring confirmation. Although sensitivity analyses suggest that patients included in this study are representative of the whole cohort, the true prevalence of PT dysfunction among patients with COVID-19 needs to be substantiated in prospective studies.

In summary, SARS-CoV-2 infection causes an early and specific dysfunction of the kidney PT characterized by LMW proteinuria, defective tubular handling of uric acid and phosphate, and neutral aminoaciduria. These transport defects are associated with structural and molecular alterations of PT cells, and detection of particles resembling coronaviruses. The presence of hypouricemia and inappropriate uricosuria is associated with disease severity and outcome. These data provide novel insights into the pathophysiology of COVID-19 and open perspectives on biomarkers of disease severity.

METHODS
Study design and patients
The very first patient with COVID-19 was admitted to our hospital on February 23, 2020. All consecutive adult patients, admitted between February 23, 2020 and April 18, 2020, at Cliniques universitaires Saint- Luc (CUSL), Brussels, Belgium with a SARS-CoV-2–associated pneumonia were enrolled in a prospective registry. The diagnosis was based on a positive SARS-CoV-2 real-time reverse transcription polymerase chain reaction (RT-PCR) analysis on nasopharyngeal swab or broncho-alveolar lavage combined with suggestive abnormalities on chest X-ray or computed tomography.

As the number of cases exponentially increased in March 2020, an additional 7 units of 20 beds were dedicated to COVID-19 to accommodate the influx of patients. They were all staffed with 2 fellows and 2 senior physicians from internal medicine or a related discipline (pulmonology, nephrology, cardiology, hepatogastroenterology, hematology, oncology, geriatrics). The infectious disease specialists supervised the general management and provided continuous expert advice.

As the pandemic progressed, we realized that routine urinalysis showed proteinuria of unknown mechanism in around 80% of

patients with COVID-19 already upon admission. This prompted us to subsequently order specific urinalyses in 49 patients with documented SARS-CoV-2 infection hospitalized at the Cliniques universitaires Saint-Luc between March 31, 2020 and April 18, 2020 (Supplementary Figure S1). Patients on kidney replacement therapy at the time of admission (hemodialysis, peritoneal dialysis, or kidney transplantation) were not included in this study. During the study period, 68 consecutive patients with SARS-CoV-2 infection were admitted to our institution.

The standard treatment for patients hospitalized for COVID-19 at that time included 400 mg hydroxychloroquine twice daily on the first hospital day, then 200 mg twice daily for 4 additional days in patients without contraindication, as recommended by the Belgian COVID-19 interim guidelines. Patients were followed until death, or the end of study follow-up on May 22, 2020.

The study was conducted in accordance with the World Medical Association's Declaration of Helsinki; the Belgian law related to experiments in humans dated May 7, 2004; the General Data Protection Regulation 2016/679; and the Belgian law of July 30, 2018 regarding the protection of personal data. The Ethical Review Board of Cliniques universitaires Saint-Luc/UCLouvain approved the study and waived the requirement to obtain informed consent based on the observational design.

Data collection and definitions

The following data were extracted from electronic medical records: demographics, symptoms at admission, unit where the patient was hospitalized first (intensive care unit vs. conventional unit), vital signs, biological and imaging data, and outcome. We recorded routine biological data obtained at admission, as well as the nadir lymphocyte count, and the peak values for highly sensitive C-reactive protein, lactate dehydrogenase, and D-dimers during hospitalization. Dipstick urinalysis (glucose, proteins) was performed at the time of admission. The frequent observation of abnormal positive dipstick proteinuria in the first patients prompted subsequent measurement of urinary levels of electrolytes, proteins, albumin, creatinine, β_2-microglobulin, and eventually amino acids for consecutive patients during hospitalization. Data were checked by 3 physicians (AW, MP, JM) and reviewed in collaboration with a fourth one (MJ).

Lab measurements were performed, unless otherwise mentioned, on an automated Roche Cobas 8000 analyzer, equipped with modules ISE, c702, c502, and e602 (Roche Diagnostics, Rotkreuz, ZG, Switzerland), or a UC3500 automated urine analyzer (Sysmex, Norderstedt, Germany). Urinary levels of β_2-microglobulin were expressed as a concentration, using an upper limit of normal of 0.3 mg/l (mean $\pm$ 2 SD in healthy subjects).[44] In our cohort, the urinary concentration of β_2-microglobulin closely correlated with urinary β_2-microglobulin-to-creatinine ratio (Spearman's $r = 0.91$, 95% confidence interval 0.84–0.95, $P < 0.001$). The pH of urine samples was >5.5, a level at which degradation of urinary β_2-microglobulin does not occur.[44]

Acute kidney injury was defined according to Kidney Disease: Improving Global Outcomes (KDIGO), as an increase in serum creatinine of $\geq$0.3 mg/dl (26.5 μmol/l) during hospitalization.[45] Hypophosphatemia was defined as a serum phosphate level <0.81 mmol/l, and hypouricemia as a serum uric acid level below 2.5 mg/dl. Inappropriate uricosuria and phosphaturia were defined as fractional excretion (FE) of uric acid >10% in patients with hypouricemia, or fractional excretion of phosphate (FE_{PO4}) >20% in those with hypophosphatemia.[24]

SARS-CoV-2 polymerase chain reaction

SARS-CoV-2 RNA detection in nasopharyngeal swabs was performed using COVID-19 genesig RT-PCR assay (Primerdesign Ltd, Chandler's Ford, UK) in a LightCycler 480 instrument (Roche Diagnostics, Mannheim, Germany). Primers and probe of this assay target the RNA-dependent RNA polymerase (RdRp) gene. A test with a cycle threshold less than 40 was considered positive.

Urine amino acids

Aminoaciduria was analyzed in only a subset of patients because (i) it requires nonautomated, manual preparation of samples, with a potential risk of contamination for lab technicians; (ii) the method is labor intensive and time consuming, requiring $\sim$270 minutes for each run, followed by additional time for data extraction. Urine amino acids were quantified by ion exchange chromatography with post column derivatization with Ninhydrin using a Biochrom 30 amino acid analyzer (Cambridge, England) in the routine workflow of the Biochemical Genetics laboratory (Cliniques universitaires Saint-Luc UCLouvain). Amino acid excretion was normalized to creatinine (in mmol/mol creat).

Antibodies and reagents

The following antibodies were used: rabbit anti-human Gc-globulin (also known as VDBP, A0021, Dako, Glostrup, Denmark); mouse anti-human ACE2 (AMAB91262, Sigma/Merck, Darmstadt, Germany); rabbit anti-human ACE2 (AF933, R&D); rabbit anti-human AQP1 (ab2219, Millipore); sheep anti-LRP2 (gift from P. Verroust and R. Kozyraki, INSERM, Paris, France); rabbit anti-human UP1 (A0257, Dako); and rabbit anti-human LMW proteins (A0126, Dako).

Immunoblot

Sodium dodecylsulfate-polyacrylamide gel electrophoresis and immunoblot were performed as previously described.[46] Urine samples were thawed on ice, diluted in Laemmli buffer, and proteins separated by sodium dodecylsulfate-polyacrylamide gel electrophoresis (7.5%, 12% or 16% acrylamide slabs) in non-reducing conditions. The volume of urine loaded in each lane was normalized for creatinine concentration. After blotting onto nitrocellulose and blocking, membranes were incubated overnight at 4 °C with primary antibody, washed, incubated with peroxidase-labeled secondary antibody, and visualized with enhanced chemiluminescence (ECL, Pierce, Aalst, Belgium).

Pathologic evaluation

Pathologic evaluation was performed on kidney samples obtained from autopsies of 6 COVID-19 cases. All specimens were well preserved without autolysis, and the postmortem interval was less than 6 hours. None of the patients received an antiviral or nephrotoxic drug. Sections of formalin-fixed paraffin-embedded blocks were stained with hematoxylin and eosin, periodic acid–Schiff, Masson trichrome, and Perls staining in all cases. Stained sections were evaluated for the number of total and sclerotic glomeruli; extent of interstitial fibrosis and tubular atrophy; presence of tubular lesions; alterations of the brush border; intra-luminal debris; vacuolization of tubular cells; erythrocytes aggregates; glomerular lesions; and interstitial inflammation.[16] All kidney sections were evaluated by an experienced kidney pathologist.

Electron microscopy

For electron microscopy, kidney samples obtained at autopsy from patients deceased from COVID-19 were fixed in 2.5% glutaraldehyde in 0.1 M cacodylate buffer (pH 7.3) overnight. After rinsing in 0.1 M cacodylate buffer, kidney samples were post-fixed in 1% osmium tetroxide in cacodylate buffer for 40 minutes at room temperature, washed, and then stained with aqueous uranyl acetate for 1 hour at room temperature. After dehydration through a graded series of ethanol, samples were infiltrated and embedded in Epon812 (Sigma, Buchs, Switzerland) at 60 °C for 28 hours. Next, 350-nm semi-thin sections were cut with a Leica EM FCS ultra-microtome (Leica Microsystem, Wetzlar, Germany) and stained with toluidine blue, followed by image acquisition by a Slidescanner (Zeiss Axio Scan.Z1, Jena, Germany) using 40× Plan Apochromat objective and image processing with ImageJ. Next, 60-nm ultra-thin sections were collected onto formvar-coated copper grids, stained with lead phosphate dilution in water, and analyzed in an electron microscope (Philips CM100, Philips Electron Optics, Eindhoven, The Netherlands) at 80kV. The sample processing and image acquisition for toluidine blue staining and transmission electron microscopy were performed at the Center for Microscopy and Image Analysis of the University of Zurich (Zurich, Switzerland).

Immunostaining

Immunostaining was performed on formaldehyde-fixed paraffin-embedded sections of normal human kidney and kidney from patients with active COVID-19, using a sequential staining protocol as described previously.[46] Paraffin blocks were sectioned into consecutive 5-μm-thick slices on Superfrost Plus glass slides (Thermo Fisher Scientific, Merelbeke, Belgium). Before staining, slides were deparaffinized in decreasing concentrations of ethanol, and antigen retrieval was performed by incubating in sodium citrate buffer (1.8% 0.1M citric acid, 8.2% 0.1M sodium citrate, in distilled water, pH 6.0) in a water bath for 30 minutes. The sections were blocked with phosphate-buffered saline containing 5% bovine serum albumin, and incubated for 1 hour with primary antibodies. After 3 phosphate-buffered saline rinses, fluorophore-conjugated Alexa secondary antibodies (Invitrogen, Carlsbad, CA) were applied for 30 minutes. Negative controls were performed by omitting the primary antibody. Sections were subsequently mounted in ProLong Gold DAPI Antifade reagent (Invitrogen) and analyzed on a Zeiss LSM800 confocal microscope (Carl Zeiss, Jena, Germany), using ×20/0.8 Plan-Apochromat (Carl Zeiss). Quantitative image analysis was performed using Zen 2 (blue edition) software (Carl Zeiss) by randomly selecting 5 visual fields per slide that included at least 3 to 5 PTs, using constant setting parameters (i.e., pinhole, laser power, and offset gain and detector amplification below pixel saturation). URAT1 and B⁰AT1 staining were obtained from the Human Protein Atlas.[47,48]

Microdissection of mouse renal tubules, quantitative reverse transcription PCR, and interactome

The segmental expression of specific markers in mouse kidney was performed as described.[49] Kidneys of C57BL6J mice were digested with type-2 collagenase, and tubules were isolated manually according to the morphologic differences, before lysis in RNA extraction buffer from RNAqueous Total RNA Isolation Kit (Invitrogen, Carlsbad, CA). Quantitative reverse transcription PCR analysis was performed on pools of ∼70 isolated renal tubules.

Total RNA was extracted from segments with RNAqueous^R kit (Applied Biosystems, Life Technologies, Darmstadt, Germany). One μg of RNA was used to perform the reverse transcriptase reaction with iScript cDNA Synthesis Kit (Bio-Rad, Temse, Belgium).

Changes in mRNA levels of the target genes were determined by relative quantitative RT-PCR with a CFX96 Real-Time PCR Detection System (Bio-Rad) using iQ SYBR Green Supermix (Bio-Rad). The analyses were performed in duplicate with 100 nM of both sense and anti-sense primers in a final volume of 20 μL using iQ SYBR Green Supermix (Bio-Rad). Specific primers were designed using Primer3 (Supplementary Table S11). PCR conditions were 95 °C for 3 minutes, followed by 40 cycles of 15 seconds at 95 °C, and 30 seconds at 60 °C. The PCR products were sequenced with the BigDye terminator kit (Perkin Elmer Applied Biosystems, Schwerzenbach, Switzerland) using an ABI3100 capillary sequencer (Perkin Elmer Applied Biosystems). The efficiency of each set of primers was determined by dilution curves (Supplementary Table S11). The relative changes in targeted genes over Gapdh mRNAs were calculated using the $2^{-\Delta\Delta Ct}$ formula.

The connectivity network of the interactions between human SLC6A19 (B⁰AT1) and other proteins, including the SARS-CoV-2 receptor ACE2 and the related protein TMEM27 (collectrin), was established using the STRING (Search Tool for the Retrieval of Interacting Genes/Proteins) database.[50]

Statistical analysis

Results are presented as mean ± SD or median (IQR) for continuous variables and as numbers and proportions for categorical variables. Continuous variables were expressed in their natural units without standardization. Comparisons between groups were performed using an unpaired t test, the Wilcoxon rank-sum (Mann-Whitney) test, or the χ^2 test, as appropriate. Spearman's rank test was performed to assess the correlation between serum uric acid level and urinary fractional excretion of uric acid.

Time-to-event analyses were performed using Cox proportional hazard regressions (where events were defined as the need for invasive mechanical ventilation or death) and a competing risk approach. In the latter, the hazard ratio for invasive mechanical ventilation and its 95% confidence interval were estimated by including each specific PT defect and baseline characteristics as covariates and by considering death and discharge as competing events. Multivariable time-to-event analyses have been adapted to adjust for pre-specified relevant covariates including age, gender, baseline lymphocyte count, lactate dehydrogenase, and highly sensitive C-reactive protein levels. Collinearity between variables was quantified using variance inflation factors, and variance inflation factors >10 suggested excessive correlation between variables.

All statistical analyses were performed using GraphPad Prism (version 8.0) or Stata (version 16.0) software. All tests were 2-tailed, and a P value < 0.05 was considered significant.

AUTHOR CONTRIBUTIONS

AW, OD, MJ, and JM designed the study; AW, LB, MP, AP, JDG, HY, LP, JCY, LG, XW, PFL, and JM took care of the patients; AW, MP, and JM collected clinical data; GS and SA performed postmortem examinations; JD, OD, and JM assessed and interpreted urine amino acids; AS performed and interpreted SARS-CoV-2 PCR; ZC, SEM, OD, and JM performed, supervised, and analyzed experiments; JM performed statistical analyses. Each author contributed important intellectual content during manuscript drafting or revision and agrees to be personally accountable for the individual's own contributions and to ensure that questions pertaining to the accuracy or integrity of any portion of the work, even one in which the author was not directly involved, are appropriately investigated and resolved, including with documentation in the literature if appropriate.

SUPPLEMENTARY MATERIAL

Supplementary File (PDF)

Figure S1. Flowchart of the study.

Figure S2. Presence of proximal tubule dysfunction signs at the individual level in patients with COVID-19.

Figure S3. Low-molecular-weight proteinuria in patients with COVID-19 and controls.

Figure S4. Expression of ACE2 in the proximal tubule and interaction with solute transporters.

Figure S5. Proximal tubule lesions in the kidneys of patients with COVID-19.

Table S1. Baseline characteristics and treatment of patients who underwent routine versus specific urinalysis.

Table S2. Characteristics of COVID-19 patients for whom urine was tested for the presence of LMW proteins by immunoblot (Figure 1d).

Table S3. Urinary concentration of amino acids in patients with COVID-19.

Table S4. Characteristics of COVID-19 patients with versus without elevated urinary β_2-microglobulin.

Table S5. Characteristics of COVID-19 patients with and without hypouricemia and inappropriate uricosuria.

Table S6. Characteristics of COVID-19 patients with versus without hypophosphatemia and inappropriate phosphaturia.

Table S7. Characteristics of COVID-19 patients with versus without aminoaciduria.

Table S8. Cox and competing risks regressions for time to invasive mechanical ventilation according to the presence of proximal tubule dysfunction.

Table S9. Characteristics of COVID-19 patients with postmortem examination of the kidneys.

Table S10. Pathologic evaluation of kidneys from patients with COVID-19.

Table S11. Mouse primer pairs for gene expression analysis.

REFERENCES

1. Acter T, Uddin N, Das J, et al. Evolution of severe acute respiratory syndrome coronavirus 2 (SARS-CoV-2) as coronavirus disease 2019 (COVID-19) pandemic: a global health emergency. *Sci Total Environ*. 2020;730:138996.
2. Wu Z, McGoogan JM. Characteristics of and important lessons from the Coronavirus Disease 2019 (COVID-19) outbreak in China: summary of a report of 72 314 cases from the Chinese Center for Disease Control and Prevention. *JAMA*. 2020;323:1239–1242.
3. Guan WJ, Ni ZY, Hu Y, et al. Clinical characteristics of Coronavirus Disease 2019 in China. *N Engl J Med*. 2020;382:1708–1720.
4. Li W, Moore MJ, Vasilieva N, et al. Angiotensin-converting enzyme 2 is a functional receptor for the SARS coronavirus. *Nature*. 2003;426:450–454.
5. Hamming I, Timens W, Bulthuis ML, et al. Tissue distribution of ACE2 protein, the functional receptor for SARS coronavirus. A first step in understanding SARS pathogenesis. *J Pathol*. 2004;203:631–637.
6. Yan R, Zhang Y, Li Y, et al. Structural basis for the recognition of SARS-CoV-2 by full-length human ACE2. *Science*. 2020;367:1444–1448.
7. Lan J, Ge J, Yu J, et al. Structure of the SARS-CoV-2 spike receptor-binding domain bound to the ACE2 receptor. *Nature*. 2020;581:215–220.
8. Diao B, Wang C, Wang R, et al. Human kidney is a target for novel severe acute respiratory syndrome Coronavirus 2 (SARS-CoV-2) infection. *medRxiv*. https://doi.org/10.1101/2020.03.04.20031120.
9. Naicker S, Yang CW, Hwang SJ, et al. The novel Coronavirus 2019 epidemic and kidneys. *Kidney Int*. 2020;97:824–828.
10. Cheng Y, Luo R, Wang K, et al. Kidney disease is associated with in-hospital death of patients with COVID-19. *Kidney Int*. 2020;97:829–838.
11. Pei G, Zhang Z, Peng J, et al. Renal involvement and early prognosis in patients with COVID-19 pneumonia. *J Am Soc Nephrol*. 2020;31:1157–1165.
12. Li Z, Wu M, Yao J, et al. Caution on kidney dysfunctions of COVID-19 patients. *medRxiv*. https://doi.org/10.1101/2020.02.08.20021212.
13. Gross O, Moerer O, Weber M, et al. COVID-19-associated nephritis: early warning for disease severity and complications? *Lancet*. 2020;395:e87–e88.
14. Tay MZ, Poh CM, Rénia L, et al. The trinity of COVID-19: immunity, inflammation and intervention. *Nat Rev Immunol*. 2020;20:363–374.
15. Puelles VG, Lütgehetmann M, Lindenmeyer MT, et al. Multiorgan and renal tropism of SARS-CoV-2. *N Engl J Med*. 383:590–592.
16. Su H, Yang M, Wan C, et al. Renal histopathological analysis of 26 postmortem findings of patients with COVID-19 in China. *Kidney Int*. 2020;98:219–227.
17. Farkash EA, Wilson AM, Jentzen JM. Ultrastructural evidence for direct renal infection with SARS-CoV-2. *J Am Soc Nephrol*. 2020;31:1683–1687.
18. Smith KD, Akilesh S, Alpers CE, Nicosia RF. Am I a Coronavirus? *Kidney Int*. 2020;98:506–507.
19. Miller SE, Brealey JK. Visualization of putative coronavirus in kidney. *Kidney Int*. 2020;98:231–232.
20. Goldsmith CS, Miller SE, Martines RB, et al. Electron microscopy of SARS-CoV-2: a challenging task. *Lancet*. 2020;395:e99.
21. Revel MP, Parkar AP, Prosch H, et al. COVID-19 patients and the radiology department—advice from the European Society of Radiology (ESR) and the European Society of Thoracic Imaging (ESTI). *Eur Radiol*. 2020;30:4903–4909.
22. Kleta R, Romeo E, Ristic Z, et al. Mutations in SLC6A19, encoding B0AT1, cause Hartnup disorder. *Nat Genet*. 2004;36:999–1002.
23. Singer D, Camargo SM. Collectrin and ACE2 in renal and intestinal amino acid transport. *Channels (Austin)*. 2011;5:410–423.
24. van der Wijst J, Belge H, Bindels RJM, Devuyst O. Learning physiology from inherited kidney disorders. *Physiol Rev*. 2019;99:1575–1653.

25. Nielsen R, Christensen EI, Birn H. Megalin and cubilin in proximal tubule protein reabsorption: from experimental models to human disease. *Kidney Int*. 2016;89:58–67.
26. Forster IC, Hernando N, Biber J, Murer H. Phosphate transporters of the SLC20 and SLC34 families. *Mol Aspects Med*. 2013;34:386–395.
27. De Matteis MA, Staiano L, Emma F, Devuyst O. The 5-phosphatase OCRL in Lowe syndrome and Dent disease 2. *Nat Rev Nephrol*. 2017;13:455–470.
28. Festa BP, Chen Z, Berquez M, et al. Impaired autophagy bridges lysosomal storage disease and epithelial dysfunction in the kidney. *Nat Commun*. 2018;9:161.
29. Festa BP, Berquez M, Gassama A, et al. OCRL deficiency impairs endolysosomal function in a humanized mouse model for Lowe syndrome and Dent disease. *Hum Mol Genet*. 2019;28:1931–1946.
30. Chen Z, Luciani A, Mateos JM, et al. Transgenic zebrafish modeling low-molecular-weight proteinuria and lysosomal storage diseases. *Kidney Int*. 2020;97:1150–1163.
31. Cez A, Brocheriou I, Lescure FX, et al. Decreased expression of megalin and cubilin and altered mitochondrial activity in tenofovir nephrotoxicity. *Hum Pathol*. 2018;73:89–101.
32. Hoffmann M, Kleine-Weber H, Schroeder S, et al. SARS-CoV-2 cell entry depends on ACE2 and TMPRSS2 and is blocked by a clinically proven protease inhibitor. *Cell*. 2020;181:271–280.e8.
33. Karimian Pour N, McColl ER, Piquette-Miller M. Impact of viral inflammation on the expression of renal drug transporters in pregnant rats. *Pharmaceutics*. 2019;11:E624.
34. Ling Y, Xu SB, Lin YX, et al. Persistence and clearance of viral RNA in 2019 novel coronavirus disease rehabilitation patients. *Chin Med J (Engl)*. 2020;133:1039–1043.
35. Sun J, Zhu A, Li H, et al. Isolation of infectious SARS-CoV-2 from urine of a COVID-19 patient. *Emerg Microbes Infect*. 2020;9:991–993.
36. Monteil V, Kwon H, Prado P, et al. Inhibition of SARS-CoV-2 infections in engineered human tissues using clinical-grade soluble human ACE2. *Cell*. 2020;181:905–913.e7.
37. Kissling S, Rotman S, Gerber C, et al. Collapsing glomerulopathy in a COVID-19 patient. *Kidney Int*. 2020;98:228–231.
38. Oshiro LS, Schieble JH, Lennette EH. Electron microscopic studies of coronavirus. *J Gen Virol*. 1971;12:161–168.
39. Goldsmith CS, Tatti KM, Ksiazek TG, et al. Ultrastructural characterization of SARS coronavirus. *Emerg Infect Dis*. 2004;10:320–326.
40. Haguenau F. "Virus-like" particles as observed with the electron microscope. In: Dalton AJ, Haguenau F, eds. *Ultrastructure of Animal Viruses and Bacteriophages*. Waltham, MA: Academic Press; 1973:391–397.
41. Miller SE. Problems and pitfalls in diagnostic electron microscopy. *Microsc Microanal*. 2012;18:172–173.
42. Wu VC, Huang JW, Hsueh PR, et al. Renal hypouricemia is an ominous sign in patients with severe acute respiratory syndrome. *Am J Kidney Dis*. 2005;45:88–95.
43. Igarashi T. Fanconi syndrome. In: Avner ED, Harmon WE, Niaudet P, Yoshikawa N, eds. *Pediatric Nephrology*. Berlin Heidelberg: Springer-Verlag; 2009:1039–1067.
44. Portman RJ, Kissane JM, Robson AM. Use of beta 2 microglobulin to diagnose tubulo-interstitial renal lesions in children. *Kidney Int*. 1986;30:91–98.
45. Ostermann M, Bellomo R, Burdmann EA, et al. Controversies in acute kidney injury: conclusions from a Kidney Disease Improving Global Outcomes (KDIGO) Conference. *Kidney Int*. 2020;98:294–309.
46. Morelle J, Sow A, Hautem N, et al. Interstitial fibrosis restricts osmotic water transport in encapsulating peritoneal sclerosis. *J Am Soc Nephrol*. 2015;26:2521–2533.
47. Uhlén M, Fagerberg L, Hallström BM, et al. Proteomics. Tissue-based map of the human proteome. *Science*. 2015;347:1260419.
48. Human Protein Atlas. v15.proteinatlas.org. Accessed May 26, 2020.
49. Tokonami N, Takata T, Beyeler J, et al. Uromodulin is expressed in the distal convoluted tubule, where it is critical for regulation of the sodium chloride cotransporter NCC. *Kidney Int*. 2018;94:701–715.
50. Szklarczyk D, Gable AL, Lyon D, et al. STRING v11: protein-protein association networks with increased coverage, supporting functional discovery in genome-wide experimental datasets. *Nucleic Acids Res*. 2019;47:D607–D613.